PL-TR-
96-3020

Microtube and Composites Research

W. Hoffman

Phillips Laboratory
Propulsion Directorate (AFMC)
Edwards Air Force Base CA 93524–7048

P. B. Pollock

Hughes STX
OL-AC Phillips Laboratory
3 Antares Road
Edwards AFB CA 93524

December 1996

Final Report

APPROVED FOR PUBLIC RELEASE; DISTRIBUTION UNLIMITED.

PHILLIPS LABORATORY
Propulsion Directorate
AIR FORCE MATERIEL COMMAND
EDWARDS AIR FORCE BASE CA 93524–7048

NOTICE

When U.S. Government drawings, specifications, or other data are used for any purpose other than a definitely related Government procurement operation, the fact that the Government may have formulated, furnished, or in any way supplied the said drawings, specifications, or other data, is not to be regarded by implication or otherwise, or in any way licensing the holder or any other person or corporation, or conveying any rights or permission to manufacture, use or sell any patented invention that may be related thereto.

FOREWORD

This final technical report, entitled "Microtube and Composites Research," presents the results of an in-house study performed by OL-AC Phillips Laboratory (RKS), Edwards Air Force Base CA 93524-7048, and Hughes STX. The Project Manager for Phillips Laboratory was Dr. Wesley P. Hoffman.

WESLEY P. HOFFMAN
Project Manager

RANNEY G. ADAMS III
Public Affairs Director
97-002

STEPHEN L. RODGERS
Director
Propulsion Sciences Division

REPORT DOCUMENTATION PAGE

Form Approved
OMB No 0704-0188

1. AGENCY USE ONLY (LEAVE BLANK)	2. REPORT DATE	3. REPORT TYPE AND DATES COVERED
	December 1996	Final

4. TITLE AND SUBTITLE

Microtube and Composites Research

5. FUNDING NUMBERS

C: F04611-93-C-0005
PE: 62601F
PR: 3059
TA: 00L6

6. AUTHOR(S)

W. Hoffman
P. B. Pollock (Hughes STX)

7. PERFORMING ORGANIZATION NAME(S) AND ADDRESS(ES)

Phillips Laboratory (AFMC)
OL-AC PL/RKS
10 East Saturn Ave.
Edwards AFB CA 93524-7680

8. PERFORMING ORGANIZATION REPORT NUMBER

PL-TR-96-3020

9. SPONSORING/MONITORING AGENCY NAME(S) AND ADDRESS(ES)

10. SPONSORING/MONITORING AGENCY REPORT NUMBER

11. SUPPLEMENTARY NOTES

COSATI CODE(S): 2004; 1104

On-site Hughes STX is part of:
Hughes STX
4400 Forbes Blvd.
Lanham MD 20706

JON 305900L6 supported both in-house and contract efforts.

12a. DISTRIBUTION/AVAILABILITY STATEMENT

Approved for Public Release; Distribution Unlimited.

12b. DISTRIBUTION CODE

A

13. ABSTRACT (MAXIMUM 200 WORDS)

This technical report covers research on the properties and behavior of micron-sized tubes. The tubes in this study were made of glass, nickel, copper and silver. Diameters were in the range of 10-100 μm. Flow studies were conducted to examine the applicability of classical fluid mechanics to this flow regime. Water was flowed through the tubes, and the flow rate was measured over long periods of time. The results show that classical fluid mechanics (Hagen-Poiselle equations for laminar flow in tubes) appears to give good first-order predictions for the flow rate. One significant problem with the flow experiments was clogging of the microtubes by oxide or dirt particles. This clogging problem affected fluid flow, since the Reynolds number in this case is typically low. Gas flows did not experience the same problem. One conclusion from the flow studies is that corrosion in the system must be carefully eliminated. Even very small corrosion rates will produce contaminant particles that can obstruct flows in microtubes. Mechanical tests were also performed on metal microtubes (silver, copper) to measure tensile strength. These tests showed that the tubes generally have tensile strengths on par with data published for fine-diameter metal wires. All the investigations in this study, both fluid and mechanical, were preliminary engineering measurements only.

14. SUBJECT TERMS

microtube; tensile; flow; laminar; micron; contaminant

15. NUMBER OF PAGES

38

16. PRICE CODE

17. SECURITY CLASSIFICATION OF REPORT	18. SECURITY CLASSIFICATION OF THIS PAGE	19. SECURITY CLASSIFICATION OF ABSTRACT	20. LIMITATION OF ABSTRACT
Unclassified	Unclassified	Unclassified	SAR

TABLE OF CONTENTS

LIST OF FIGURES

LIST OF TABLES

GLOSSARY

SEM	scanning electron microscopy
STM	scanning tunneling microscopy

1.0 INTRODUCTION

This report covers the program during the period 1993 through 1995. The program has been known by at least two separate titles. Originally it was called "Advanced Composite Research" and the work statement covered the mechanical behavior of carbon-carbon composites. The program was retitled "Materials Phenomenology" in late 1993. The change of title reflected a broadening of the work statement in the program, at the request of government managers at the United States Air Force (USAF) Operating Location (OL-AC) Phillips Laboratory (PL), Propulsion Directorate, Edwards AFB, California. New activities concerning microtube technology were added to the work statement. This report covers the fluid mechanics research on microtubes and the mechanical testing of microtubes. It should be noted that work on the mechanical behavior of microdevices and the fracture of carbon-carbon composites will be published by one of the authors in a forthcoming technical report by Hughes STX. The same author has also published previous scientific papers on the fracture of carbon-carbon composites.

2.0 FLOWS IN MICROTUBES

2.1 Summary of Fluid Mechanics Experiments

A set of experiments was performed to determine if flows in microtubes could be predicted using classical fluid mechanics. This was a preliminary engineering investigation. As a result, the design of the apparatus was kept simple. The majority of the tests were conducted on commercial silica microtubes with a diameter of 10 μm and lengths in the range of 1 to 3 cm. All the microtubes were circular in cross-section. Pressure drops across the microtubes ranged from 483 to 552 kPa (70 to 80 psi), giving pressure gradients of 16 to 55 MPa/m (59 to 203 psi/in). Some tests were also performed on silica microtubes with diameters of 5, 30 and 100 μm, all in the low-pressure regime (483 to 552 kPa pressure drop across the tube length). All the liquid flow tests used distilled water as the working fluid.

High-pressure tests were also investigated, with pressure drops across the tubes ranging from 14 to 21 MPa (2000 to 3000 psi), giving pressure gradients of 467 to 2100 MPa/m (1700 to 7700 psi/in). These high-pressure tests were conducted using both gaseous argon and water as the working fluids. The microtubes for the high pressure studies were fabricated from nickel and had a diameter of 100 μm. These tubes were manufactured by an in-house laboratory program. Lengths of the tubes were in the range of 2 to 3 cm. The purpose of these tests was to check the structural integrity of the microtubes and to remove contaminants in the tubes using high-velocity flows.

The clogging of microtubes by dirt and other contaminants was a major problem. The problem primarily affected the liquid flows because the Reynolds number governing these flow conditions is small. Gas flows in microtubes generally do not have the same problem with clogging because the gas velocities are much higher. Section 2.5 (Clogging of Microtubes) discusses problems with flow obstructions caused by dirt and other contaminants.

The results of the study indicate that classical fluid mechanics gives good predictions for microtubes having diameters greater than 10 μm. The results for small-diameter microtubes are still open to question.

2.2 Experimental Procedure

Figure 1 shows the experimental arrangement for low-pressure flow studies. The water reservoir was a piece of stainless steel tubing approximately 1m in length. This tube was filled with distilled water prior to each experiment. Compressed nitrogen was applied to the top of the tube, driving the water through a filter and then into the microtube. The filter (Fisher Scientific Model 304 High Pressure Filter) consisted of a fine stainless steel mesh supporting a filter paper and was used to trap dirt particles. Originally, the intention was to use a sub-μm paper in the filter apparatus. However, it was found that very fine filter papers caused a large pressure drop. Consequently, most of the experiments used much coarser filter papers (5-μm filters) and sometimes no filter paper at all. This limitation was imposed because an 80 psi line was the only pressure source available for the initial set of experiments.

All of the stainless steel parts in the apparatus were subjected to chemical etching and cleaning treatments prior to the experiments. Care was taken to keep the distilled water free from dust contamination.

Below the filter was a T-junction. One side of the T-junction was connected to a pressure transducer. The transducer (Omega PX945-200GI transducer with PS-4E snubber) was a high-accuracy unit designed for pressures in the range of 0 to 200 psi. By placing the pressure transducer below the filter, it was possible to read the true inlet pressure to the microtube. The other end of the T-junction led to a stainless steel pressure cap holding the microtube.

The microtube was mounted through a hole in the stainless steel cap and sealed in place using epoxy glue. Care was taken to see that the glue did not enter the microtube and block the flow of water. Flow going through the microtube was collected in a small vial. The collection vial was sealed to the microtube using a silicone rubber joint at the lid of the vial. This eliminated evaporation losses as a source of error for the larger diameter microtubes (diameters of 10 μm or greater). There was no significant pressure buildup within the vial during the course of experiments. Evidently a very small air leakage was still possible past the silicone rubber seal.

The silica microtubes used in these experiments were produced commercially by Polymicro Inc. Prior to each experiment, the length of the microtube was measured with a micrometer to an accuracy of 0.002 cm, and the microtube was then epoxied in place in the stainless steel cap. Once the glue had dried, the pressure cap was screwed into the T-junction and the upper reservoir was filled with water. Gas pressure was applied to the reservoir, causing a flow of water through the microtube. After the flow had stabilized, usually within 10 to 20 sec, the collection vial was set in place and sealed with silicone rubber. This last operation was performed quickly.

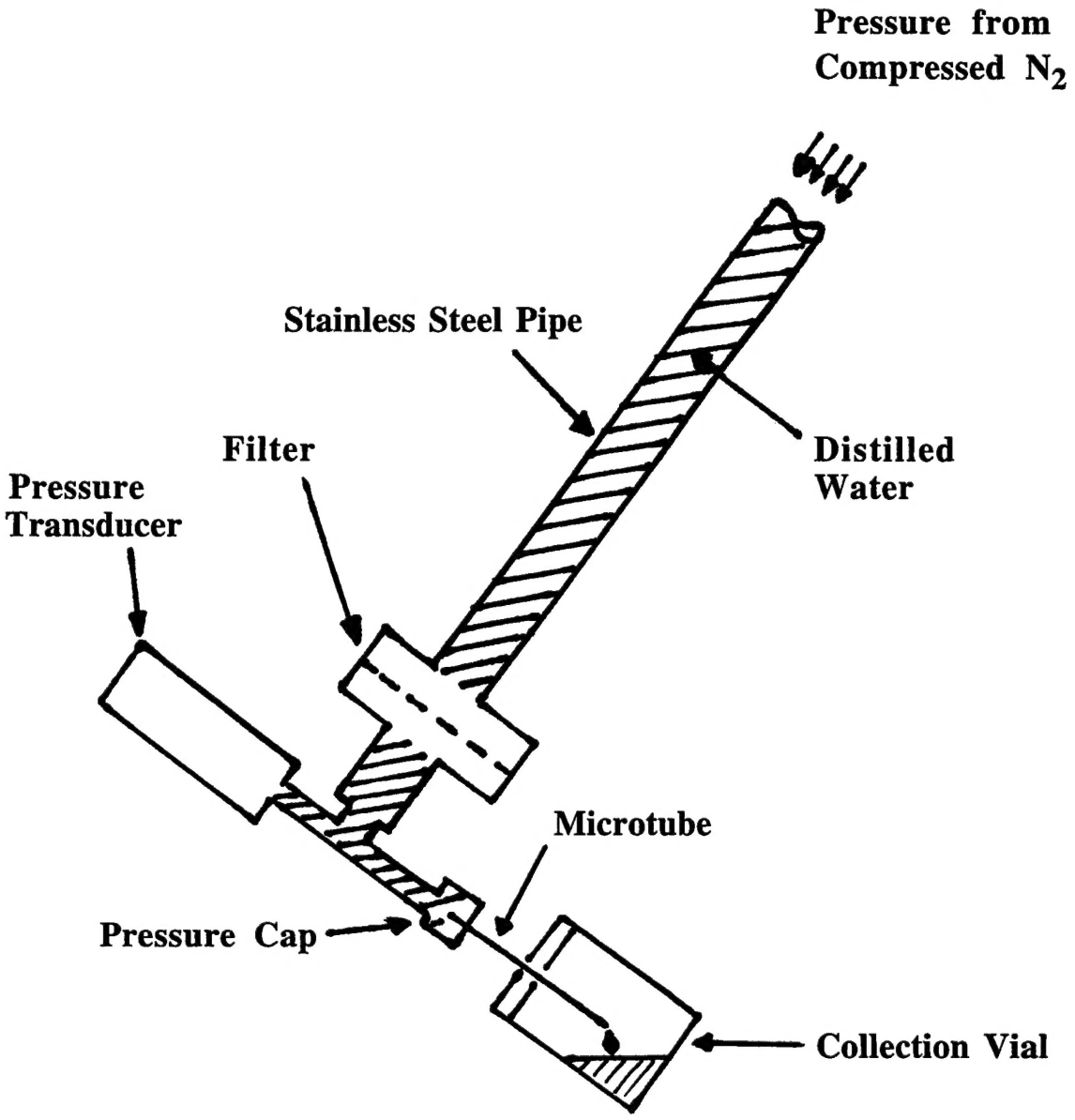

Figure 1
Flow Testing Apparatus

The experiment was left running until a reasonable amount of water had collected in the vial. At the time of termination of the experiment, the vial was quickly removed from the apparatus by breaking the silicone seal. The lid of the vial, including the silicone rubber, was removed prior to weighing the contents of the vial. It was important to accurately measure the time when the vial began collecting water and the time when the vial was removed from the apparatus.

The mass of the water could be determined accurately with a laboratory balance by determining the change in weight of the vial. The flow rate (grams per minute) was then computed by dividing the mass of water by the time duration of the experiment. Theoretical calculations normally give the flow rate in units of cubic centimeters per minute, but this was easily converted to grams per minute by multiplying by the density of water at room temperature.

2.3 Experimental Errors

Several aspects of the experimental procedure require discussion. First, the flow rate of water through the microtubes was very small, typically one or two drops per minute. This made it possible to place the collection vial on the flow apparatus between drops. Therefore there were no errors caused by the splashing of water while the vial was being placed in position.

The very small flow rates in these experiments did, however, lead to other problems. One was the evaporation of water vapor from the vial. As mentioned earlier, the solution was to carefully seal the top of the vial with silicone rubber. This prevented the escape of water vapor at the junction between the lid of the vial and the microtube.

Other potential solutions to the evaporation problem were also considered. For example, cooling the collection vial would reduce the evaporation rate of the water. However, this technique also caused condensation of moisture on the walls of the vial, leading to errors when determining the vial's weight. Another option was to use non-aqueous fluids in the experiments. Liquids having low vapor pressures at room temperature are available, e.g., certain types of hydrocarbons. However, these fluids generally have much higher viscosities than water, so their flow rates were too low to be practical. The constraints of low viscosity and ease of handling, including non-flammability, eliminated non-aqueous liquids from this preliminary study.

One of the biggest problems in the microtube experiments was clogging caused by contaminants. Long-duration experiments were often necessary to obtain accurate flow rate data. The clogging of microtubes presented a serious obstacle to the study of flows in small-diameter microtubes. This will be discussed in Section 2.5 (Clogging of Microtubes).

2.4 Experimental Results

Table 1 shows data obtained from flow tests on microtubes having diameters of 5 and 10 μm. The experimental data were lower than theoretical predictions computed by the Hagen-Poiseuille equation for laminar flow in circular pipes [Ref. 1]. The errors were in the range of 16 to 27%.

Such errors can be explained by deviations in the real diameters of the tubes. For example, if the true diameter of a microtube was 4% lower than the manufacturer's specified value, this would make the real flow rate 16% below the theoretical prediction. This expanded error comes from the Hagen-Poiseuille equation, which shows that the flow rate depends on the fourth power of the diameter.

It should be mentioned that the Reynolds number for fluid flows in microtubes is very small. For example, a 10 μm diameter microtube with an applied pressure gradient of 21.7 MPa/m (80 psi/in) has a Reynolds number of only 0.67. This calculation assumes the working fluid is water at room temperature. It follows that the flow is laminar and that the use of the Hagen-Poiseuille equation is justified for theoretical predictions.

Table 1. Data From Microtube Experiments

Diameter: 5 μm	Length: 3.32 cm (1.306 in)
	Applied Pressure: 78.50 psi
Time: 1325.0 min	Volume of Water Collected: 0.0143 g
Experimental Flow Rate:	1.08×10^5 g/min
Theoretical Flow Rate:	1.48×10^5 g/min
Diameter: 10 μm	Length: 3.02 cm (1.189 in)
Time: 5463.0 min	Applied Pressure: 77.6 psi
Experimental Flow Rate:	Volume of Water Collected: 1.0417 g
Theoretical Flow Rate:	1.91×10^4 g/min
	2.60×10^4 g/min
Diameter: 10 μm	Length: 3.32 cm (1.307 in)
	Applied Pressure: 79.93 psi
Time: 5960.6 min	Volume of Water Collected: 1.1858 g
Experimental Flow Rate:	1.99×10^4 g/min
Theoretical Flow Rate:	2.43×10^4 g/min
Diameter: 10 μm	Length: 4.00 cm (1.575 in)
	Applied Pressure: 77.7 psi
Time: 4066.0 min	Volume of Water Collected: 0.6724 g
Experimental Flow Rate:	1.65×10^4 g/min
Theoretical Flow Rate:	1.96×10^4 g/min

Experiments were also performed on microtubes with diameters of 30 and 100 μm. The data are not recorded here but, in general, the tests gave flow rates that were within 10 to 20% of the theoretical flow predictions.

It is natural to ask why the small-diameter microtubes gave greater experimental errors. The issue was studied by conducting a flow test on a 10-μm diameter microtube over an extended time period. Figure 2 plots the total mass of water accumulated in the collection vial as a function of time. The slope of this curve gives the flow rate at any instant. It is seen that the flow rate is continuously decreasing. In fact, when the experiment was continued indefinitely, the flow stopped altogether. This result appears to contradict the expected behavior. If the applied pressure, microtube length and microtube diameter are all constant, then the flow rate should also be a constant. For the flow rate to change, one of these variables must be changing. Indeed, it was shown later that the microtube diameter was reducing over time. This effect is discussed in Section 2.5 (Clogging of Microtubes).

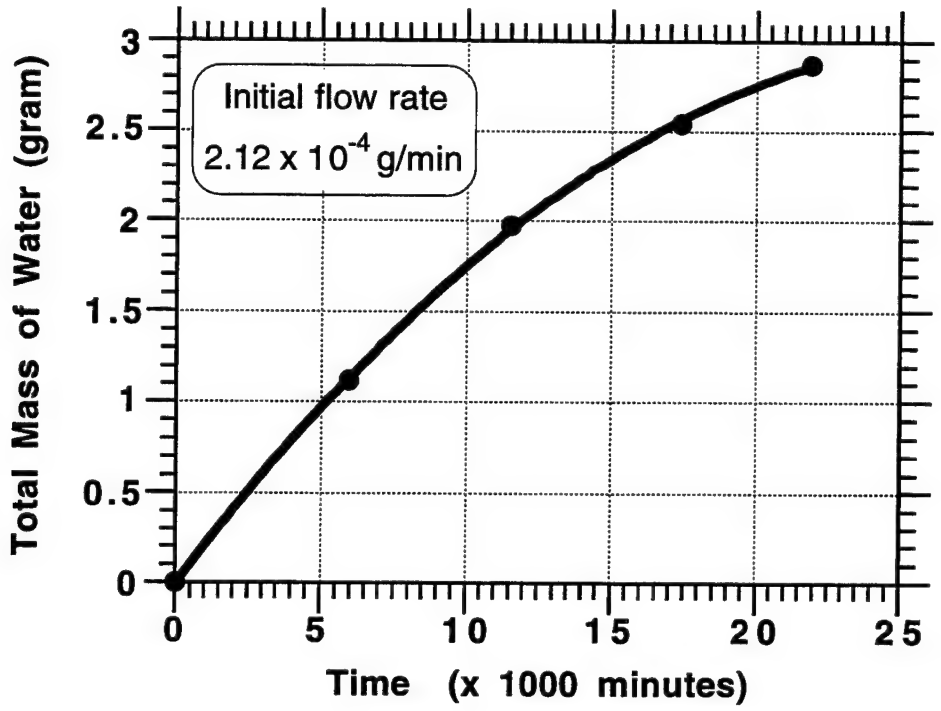

Figure 2
Long-Term Flow Experiment

It is concluded that the Hagen-Poiseuille equation does give reasonable predictions for flows in microtubes with diameters greater than 10 μm. Admittedly, the experimental errors in this preliminary study are quite high (10 to 20%), and there are some discrepancies between the experimental data and the theoretical predictions. However, plausible explanations can be found for these discrepancies; e.g., obstruction of the microtube flow by dirt particles, and errors in the microtube flow rate caused by uncertainties in the precise value of the microtube diameter. It does

not appear necessary to claim that there is a breakdown in classical fluid mechanics, at least not on the scale of these experiments (microtube diameters greater than 10 μm). However, it should be noted that this was an engineering investigation and not a precise scientific study. The aim was merely to see if reasonable estimates of the microtube flows could be predicted, so that engineering devices could be constructed for customers. That aim was achieved.

2.5 Clogging of Microtubes

The flow rate study depicted in Figure 2 showed that there was a long-term problem with microtube flows. It was discovered that the microtube cross-sectional was decreasing as the experiment progressed. Over a period of time, dirt particles were accumulating in the microtube and obstructing the flow. These particles most likely originated as rust or other surface contaminants that broke away from the walls of the stainless steel apparatus. The problem was found to be general in nature, and it extended beyond the current set of experiments. For example, one engineering application also required that water be transmitted through 100-μm diameter microtubes. Occasionally, these tubes would clog up and the flow would stop. Scanning electron microscopy (SEM) studies showed that the contamination was indeed iron oxide particles, probably originating from the stainless steel pipes that supported the microtubes. These particles were dislodged from the pipe wall, penetrated through the filtration system (or originated on the downstream side of the filter), and stopped when they met some protrusion on the microtube walls.

It should be noted that stainless steel tubes were originally selected with the intention of avoiding contamination, since this steel alloy has a high corrosion resistance. Such an approach would work well for large-scale engineering applications. However, it was discovered that for systems that operate at the microscopic scale, there is still a problem if even a tiny amount of corrosion is present.

From Figure 2, it is possible to compute the initial flow rate by drawing a tangent to the curve at the origin. This initial rate is 2.12×10^4 g/min. This is the true flow rate with no obstructions in the microtube. If, instead, the flow rate is calculated by a secant method, by joining the origin and the first data point with a straight line, the result is a flow rate of 1.96×10^4 g/min. This secant-method calculation is the result that would be obtained based on the long-duration experimental data. It follows that the true flow rate is higher than the apparent experimental value by an error of 8 to 12%. The actual magnitude of the error depends on the duration of the experiment. For larger microtubes – e.g., tubes with diameters of 30 to 100 μm – the experiments were run for much shorter time periods. Thus, the experimental error was much smaller for these larger tubes.

2.6 High-Pressure Experiments

Several high-pressure experiments were performed using nickel microtubes. These microtubes had a diameter of 100 μm and a wall thickness of 40 to 50 μm. There were two goals for the high-pressure investigation: 1) To check the structural integrity of the nickel microtubes at high

pressures, and 2) To see if high-pressure gas could push dirt particles out from the interior of the microtubes.

The nickel microtube was attached into a stainless steel tube (the method of attachment is proprietary). The microtube replaced a section of the steel tube, so that a fluid could pass from the steel pipe, through the microtube, and then back into the remaining section of the steel pipe. The front end of the stainless steel tube was connected to a high-pressure argon gas cylinder (using a pressure regulator). The rear end of the stainless steel pipe was vented to atmospheric pressure. Argon gas, or water propelled by gas pressure, was driven through the steel tube and the microtube, before being exhausted to the atmosphere. Since the stainless steel tube had a diameter of a few millimeters, the microtube was the only real obstruction to the flow. Therefore, flow rates were governed by the microtube diameter.

To check the integrity of microtube specimens, the rear end of the stainless steel pipe was capped; i.e., the atmospheric vent was closed. Consequently, the stainless steel pipe and the microtube were exposed to an internal gas pressure. The experiments were run with internal pressures ranging from 2000 to 3000 psi. At no time did the nickel microtubes experience any mechanical failures. For a microtube with a 40-μm wall thickness and diameter of 100 μm, the hoop stress, σ, in the wall is related to the internal pressure, p, by Equation 1:

$$\sigma = (\text{radius} \times \text{pressure} / \text{wall thickness}) = (50p / 40) = 1.25\ p \qquad (1)$$

The expected hoop stress is, therefore, 3750 psi for an internal pressure of 3000 psi. This hoop stress is well below the failure stress of nickel (72,000 psi), so the success of the microtubes is not surprising. However, the integrity test did show that there were no large flaws in the walls of the microtubes. Large flaws – e.g., cracks or pores with dimensions of 5 to 20 μm – would probably have produced catastrophic failure of the microtube specimens.

The second purpose of the high-pressure tests was to remove dirt particles from inside the microtubes. During the flow tests, some of the nickel microtubes became clogged by contaminants. SEM inspection showed that the primary contaminant was iron oxide, probably originating as rust particles on the walls of the stainless steel tube. One possible method to remove these flow obstructions was to push them out with high-pressure gas. However, high-pressure gas flow was not successful in re-opening the tubes. High-pressure water flow also failed as a cleaning technique. Various chemical cleaning treatments (e.g., dilute acids) were also tried, again without solving the problem. The cleaning treatments did not work because a residual population of contaminants remained, even following acid treatments. Unfortunately, acid etching could only be used for short time periods because the acid also attacked the walls of the nickel microtube. Evidently the contamination particles were able to survive this short-duration acid attack.

2.7 Suggested Improvements to Experiments

It is clear that improvements are needed in microtube technology, especially in regards to liquid flows in small-diameter tubes. These include clean-room technology, the development of improved flow rate sensors, and better measurements of microtube diameters.

2.7.1 Clean-Room Technology. Clean-room technology is needed to prevent contamination. Both the working fluid and the flow apparatus need to be isolated from dust particles. In addition, the formation of surface oxides should be prevented; e.g., elimination of water/oxygen, or the use of special corrosion-resistant materials and working fluids. It is not satisfactory to simply filter the working fluid, because filtering is usually only performed at one point in the flow system. Contaminants originating on the downstream side of the filter can still clog the microtubes. Neither is it possible to rely solely on chemical cleaning. Cleaning is certainly helpful, but fine dirt particles and contaminants will still work their way into the flow. Clean-room technology appears to be necessary if liquid flows in microtubes and micro-devices are to be successful. It should be noted that gas flows in microtubes did not experience the same problems with contaminants, perhaps because the flow velocities were much higher.

Unfortunately one problem with the clean-room approach is that the microtube is sealed from the environment. This is desirable for removing contact with contaminants. However, it also rules out valuable engineering applications; e.g., sensors that detect chemicals in an external environment.

It should be noted that the present problems with clogging of microtubes were partly a result of materials selection. Had different metal alloys, or different working fluids, been selected for the experiments, the contamination problem might have been reduced considerably. This is a lesson that has been learned for the design of future engineering applications for microtubes.

2.7.2 Improved Flow Rate Sensor. An improved sensor is needed to measure mass flow rates less than 1 μg/min. This type of sensor is essential for studying flows in microtubes with diameters less than 10 μm. There have been speculations by researchers that classical fluid mechanics may not apply to microtubes with very small diameters; e.g., it has been postulated that fluids may slip at the wall boundary, leading to higher-than-predicted flow rates. The current investigation did not study these effects. A micro-flow-rate sensor will be needed for experiments on microtubes with diameters less than 10 μm.

2.7.3 Characterization of Microtube Geometry. There is definitely a need to improve the characterization of microtube diameters and surface roughness profiles. As mentioned earlier, the flow rate is proportional to the fourth power of the microtube diameter. Hence, small errors in the measured diameter can lead to big errors in the calculations. The present investigation made some progress by applying scanning tunneling microscopy (STM) to microtube characterization. This technique is not straightforward, because STM is designed to operate on a flat scanning surface. Therefore, the hollow interior of the microtube must be filled with a solid material. One method is to use a liquid resin for impregnation of the microtube and then to cure the resin. In this way, a scan across the tube cross-section can be made. However, the method is very time consuming and needs to be perfected. It is likely that STM techniques can be adapted to characterize the inner-surface roughness of microtubes also.

3.0 TENSILE TESTING OF MICROTUBES

3.1 Summary of Tensile Testing

Mechanical testing was performed on a large number of metal microtubes. The purpose of these tests was to establish the tensile strength and stress-strain behavior of the microtubes. These data were required for engineering design purposes and were also helpful as a quality control indicator.

In general, there was a very wide scatter in the strength data for the microtubes. Two reasons are suggested for this. The first is that a large number of the microtubes were not straight. As a result, bending effects often reduced the apparent values for tensile strength. Considerable care was needed during the handling of the specimens to obtain good test results.

The second reason for data scatter was that the test technique was only designed to give approximate results. To precisely calculate the ultimate stress for a microtube, it is necessary to know the exact cross-sectional area of the specimen. Unfortunately, accurate SEM measurements were not available for the microtubes; hence, an approximate method was developed to calculate the microtube cross-sectional area based on stiffness data. The strength data in this report are suitable only for quality-control purposes and as a first-order indication of microtube properties.

This preliminary investigation showed that the metal microtubes (nickel, silver) do achieve very good tensile strengths. The strength data from the microtubes were compared with the data on metals in scientific reference books, particularly the strengths for fine-diameter metal wires [Ref. 2]. The average ultimate stress of the microtubes compared favorably with the ultimate stresses in metal wires made from corresponding types of metals.

As noted earlier, considerable care was necessary during these tests. The microtubes are fragile because of their small size. The delicate nature of the microtubes will affect their performance in some engineering applications.

3.2 Experimental Procedures

Tensile testing on microtubes was carried out using a miniature test fixture. This fixture was made using a small micro-positioner (Motor Mike unit manufactured by the Oriel Corporation). The Motor Mike device is normally used for accurate positioning of optics components. The device has a range of travel of 5.1 cm (2.0 in) and can be positioned to an accuracy of 0.1 μm. This also makes the positioner ideal as a miniature tensile testing device. The only shortcoming is that the motor drive has a limited torque; hence, very strong specimens cannot be tested. In practice, the positioner was able to test metal microtubes with diameters ranging from 10 to 100 μm and wall thicknesses of 5 to 20 μm. Carbon and polymer fibers were also tested using this device.

The micro-positioner was instrumented with a variable-speed control system and a digital position readout (Oriel Single Controller Model 18007). A 50-g load cell made by Sensotec was mounted

onto a metal bracket and attached to the micro-positioner. The bracket had a screw adjustment so that the alignment of the tensile tester could be adjusted manually.

The gripping of test specimens, such as fibers and microtubes, is an important issue. Usually specimens break at low loads if mechanical grips are used, especially for brittle materials. This is caused by stress concentrations associated with the gripping forces. For this reason, an alternative system was developed to bond the microtubes to the test device. After the micro-tester was aligned, a test specimen was carefully placed on the loading fixtures using tweezers. The specimen was then glued in place using methyl-cyanoacrylate adhesive. This attachment technique left the specimen stress-free. Subsequent testing showed that there was no significant deformation of the glue joints during tensile testing.

Figure 3 shows a magnified photograph of a microtube ready for testing. The horizontal metal tab on the left side of the picture is the end of the load cell, while the large metal fixture on the right is part of the micro-positioning table. During testing, the tab and the fixture move apart, placing the microtube in tension. The glue joint that bonds the microtube is transparent and cannot be seen in Figure 3. Scratch marks are clearly visible on both of the load fixtures where the specimen was mounted. These scratches were caused by cleaning procedures. Before a new specimen was installed, excess glue was carefully removed from each load fixture with a razor blade.

The scratches caused no problems to the test technique. It can be seen in Figure 3 that the microtube is not straight. This was a common problem with microtube specimens. During testing,

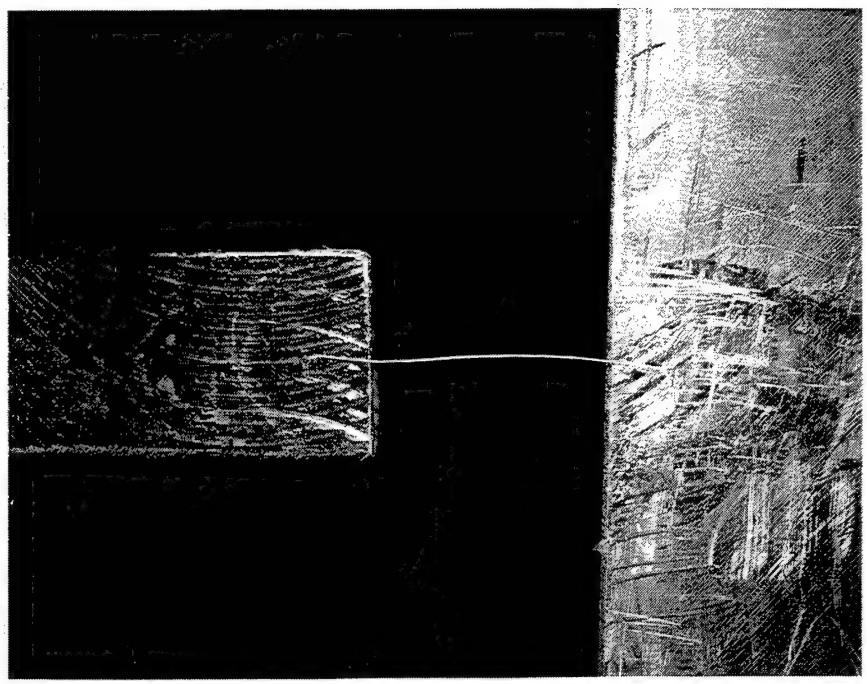

Figure 3
Tensile Testing of Microtube

the specimens were pulled into a straighter shape by the tensile load, but this sometimes caused premature failure because of bending stresses.

The test procedure itself was very straightforward. Once the specimen was prepared for testing, the micro-tester was turned on. Tensile extension was run at a relatively slow rate of 1000 microstrain/min. A typical test took 3 to 5 min. Data were recorded manually in a notebook as the experiment progressed, without interrupting the test. Plots of load versus extension were converted into stress versus strain according to the method described in Section 3.4 (Analysis of Tensile Test Data).

3.3 Standards and Calibration

The displacement of the micro-tester was checked using a micrometer and found to be accurate. The calibration of the Sensotec load cell was checked by hanging a small weight from the cell, noting the reading, and then confirming the force measurement using a high-accuracy laboratory balance.

The operation of the micro-tester was checked by running tensile tests on carbon fibers with a known stiffness. The modulus data for P-55 carbon fibers were found to be 45 Msi, 59.5 Msi, 78.7 Msi and 63.0 Msi. The literature reported values for the P-55 stiffness of 48 Msi and 55.1 Msi. Therefore, the experimental tests were in good agreement with the expected values. A reasonable scatter in the actual moduli of the fibers is normal. The experimental stress-strain curves for the P-55 fibers also showed that the modulus increased as the applied stress increased, an unusual behavior that is characteristic of carbon fibers.

An independent check was made of the compliance of the micro-tester. The compliance is the inverse of the stiffness and, ideally, any test device should have zero compliance. It was found that the correction to the stiffness data of test specimens, because of the non-zero compliance of the micro-tester, was very small. Errors caused by the compliance correction were usually less than 2%.

3.4 Analysis of Tensile Test Data

Figure 4 illustrates a stress-strain test for a copper microtube. The horizontal axis is strain, computed by dividing the extension of the microtube by its original length. The vertical axis is the applied force measured by the load cell. All of the tensile test plots for the microtubes showed an initial region of nonlinear response. This occurred as the microtube was being stretched into a straight shape. Usually, there followed a straight response to failure, as seen in Figure 4. The slope of this straight line was measured to be 30.72 N. Theoretically, this slope should be equal to EA, where E is the Young's modulus of the metal in the microtube and A is the cross-sectional area. Therefore, knowing that the microtube in Figure 4 is made of copper, with a modulus of E = 129.8 GPa, it follows that the cross-sectional area $A = 2.37 \times 10^{-10}$ m^2. This is the method used to determine the cross-sectional area of the microtubes, in the absence of accurate SEM data. It is

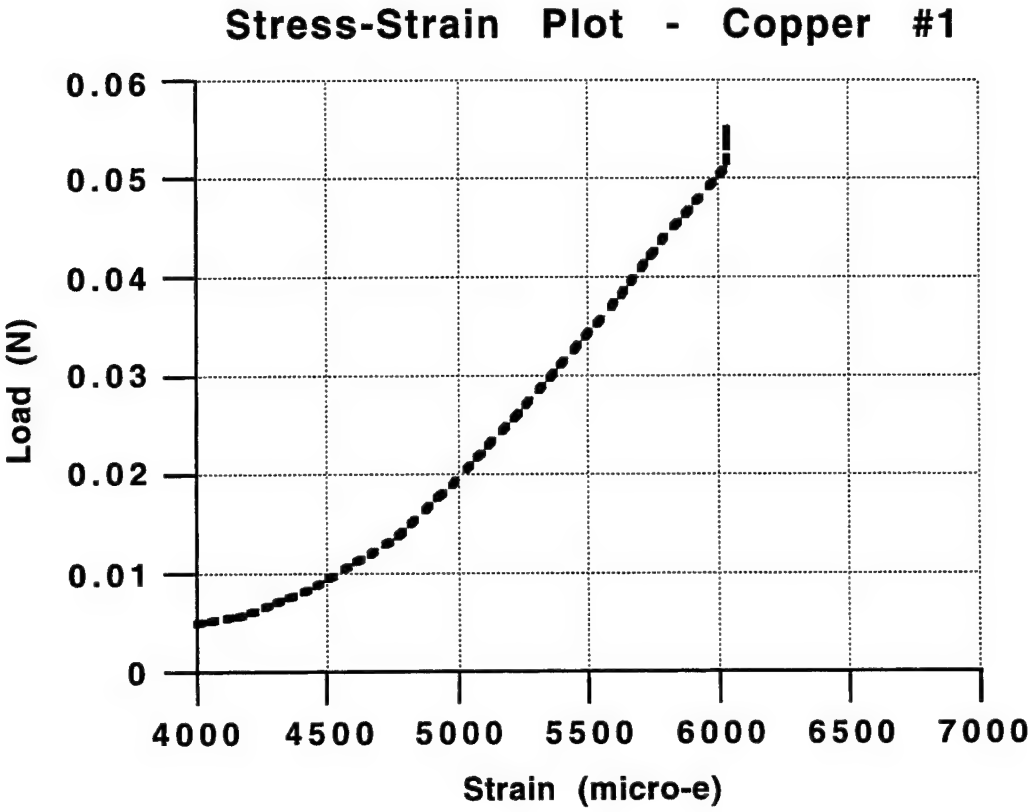

$$\frac{0.06 \text{ N}}{(6325 - 4372) \times 10^{-6}} = EA = 30.72 \text{ N}$$

E (copper) = 129.8 GPa

Therefore A = 2.367×10^{10} sq. ms

Ultimate Stress = 2.34×10^{8} Pa

strength performance factor = 80% of annealed copper wire

Figure 4
Microtube Stress-Strain Calculation

clear that this approach is based on two fairly broad assumptions: that the strain is uniform along the length of the microtube and that the microtube has a uniform geometry. If necking occurs at high loads, this analysis will contain errors. Fortunately, the majority of the specimens had stress-strain plots that were reasonably linear to failure (after an initial nonlinear response at low loads).

With the cross-sectional area now estimated, the ultimate stress of the microtube can be calculated. The ultimate stress is simply the failure load divided by the area. Tables 2 and 3 present data for a large number of microtubes made of copper and silver. A strength performance factor was calculated for each microtube. This was found by dividing the ultimate stress of the microtube by the strength of a fine-diameter wire made of the same metal. Going back to the example in Figure 4, the ultimate stress of the copper microtube was found to be 0.234 GPa. The ultimate stress of an annealed copper wire is 0.300 GPa. The strength performance factor for this specimen is 0.234/0.300 = 78%. A strength performance factor of 100% indicates that the microtube has the same performance as a fine-diameter metal wire.

Table 2. Batch 1: 10-μm Diameter Copper Microtubes

Specimen	Ultimate Stress (GPa)	Strength Performance Factor
#1, length = 1.66 cm	0.234	79%
#2, length = 1.71 cm	0.337	114%
#3, length = 1.69 cm	0.179	61%
#4, length = 1.74 cm	0.234	80%
#5, length = 1.74 cm	0.236	80%
#6, length = 1.93 cm	0.207	70%
#7, length = 1.96 cm	0.166	56%
#8, length = 1.95 cm	0.217	74%
Average Strength:	0.226 GPa	76%
Standard Deviation:	0.5 GPa	

Table 3. Batch 2: 10-μm Diameter Copper Microtubes

Specimen	Ultimate Stress (GPa)	Strength Performance Factor
#1, length = 1.40 cm	0.835	278%
#2, length = 0.45 cm	0.718	239%
#3, length = 0.63 cm	0.176	25%
#4, length = 1.01 cm	0.409	136%
#5, length = 0.64 cm	0.642	214%
#6, length = 0.64 cm	0.360	120%
#7, length = 0.91 cm	0.294	98%
#8, length = 0.93 cm	0.494	164%
#9, length = 0.68 cm	0.224	75%
#10, length = 0.68 cm	0.353	118%
#11, length = 0.68 cm	0.300	100%
Average Strength:	0.427 GPa	142%
Standard Deviation:	0.23 GPa	

3.5 Test Results

Tables 2 through 4 show data for copper and silver microtubes. Samples of the stress-strain plots for some of these specimens are included in Appendix A. The microtubes in this study had wall thicknesses ranging from 0.5 to 3.0 μm. The copper microtubes had a diameter of 10 μm, and the silver microtubes had a diameter of 100 μm.

It can be seen in Tables 2 and 3 that the two batches of copper microtubes had significantly different properties, with the second batch being almost twice as strong as the first. The most likely explanation is processing variations from batch to batch. The microtubes are usually made from circumferential layers of metal. Therefore, it is possible to get a buildup of internal stresses at the interface between consecutive layers. The magnitude of these stresses depends on the processing conditions during the microtube fabrication. Evidently, the Batch 2 microtubes had low internal stresses and, therefore, exhibited much higher tensile strengths. The data in Tables 3 and 4 show that the microtubes did indeed achieve good mechanical strengths. The strength performance factor for the copper microtubes (Batch 2) was 142%, and the strength performance factor for the silver microtubes was 114%.

Table 4. Batch 1: 100-μm Diameter Silver Microtubes

Specimen	Ultimate Stress (GPa)	Strength Performance Factor
#1, length = 1.98 cm	0.302	104%
#2, length = 1.98 cm	0.326	112%
#3, length = 2.00 cm	0.352	121%
#4, length = 2.02 cm	0.278	96%
#5, length = 1.74 cm	0.502	173%
#6, length = 1.74 cm	0.393	136%
#7, length = 1.82 cm	0.562	163%
#8, length = 1.85 cm	0.365	126%
#9, length = 1.88 cm	0.469	162%
#10, length = 1.89 cm	0.446	154%
#11, length = 1.89 cm	0.302	104%
#12, length = 1.93 cm	0.247	85%
#13, length = 1.94 cm	0.253	87%
#14, length = 1.95 cm	0.399	136%
#15, length = 1.94 cm	0.357	123%
#16, length = 1.96 cm	0.376	129%
#17, length = 1.95 cm	0.232	80%
#18, length = 1.98 cm	0.359	134%
#19, length = 2.00 cm	0.310	107%
#20, length = 2.02 cm	0.296	102%
#21, length = 2.00 cm	0.293	101%
#22, length = 2.03 cm	0.282	97%
#23, length = 2.04 cm	0.324	112%
#24, length = 2.05 cm	0.228	78%
#25, length = 2.06 cm	0.192	66%
#26, length = 2.08 cm	0.228	78%
Average Strength:	0.334 GPa	114%
Standard Deviation:	0.090 GPa	

4.0 CONCLUSIONS

Microtubes are finding diverse applications: micro-waveguides and IR-filters, channels for gas separation, conduits for bacterial growth and transport, micro-reactors, and micro-sensors. Two of the key engineering issues associated with microtubes are: how can fluid flows be predicted in microtubes, and do the microtubes have good structural integrity?

To address the first question a preliminary set of flow experiments was performed. The results show that flow rates can be predicted with good accuracy for microtubes with diameters greater than 10μ. The predictions were computed using the equation for laminar flow in a circular pipe, and errors were typically less than 10%. This result is expected to be valid for both liquids and gases. Since this was an engineering investigation, high-accuracy measurements of the flow rate amd microtube diameter were not performed. Hence it was not possible to assess the limitations of classical fluid mechanics theory.

In general there were few problems with gas flows in microtubes. However, liquid flows in microtubes encountered problems due to clogging by contaminants. Liquid typically have a low Reynolds number. Hence flow velocities are small and contaminant particles can build up on the tube walls. The flow obstruction problem was most severe for microtubes with diameters less than 20μ. Obvious solutions, based on engineering experience with macroscopic systems, do not always work. For example, stainless steel is considered corrosion-free at the macroscopic scale. However, it was found that tiny iron-oxide particles do break free from the walls of stainless steel components. These particles will lodge on the walls of a microtube over a long period of time (hours or days), and obstruct the flow. Thus it is necessary to pay particular attention to issues such as corrosion, materials compatibility, and clean-room technology.

To address the second issue of structural integrity, a series of tensile tests was performed on microtube specimens. These tests have shown that microtubes achieve strengths which are roughly comparable to ultimate stress data for fine-diameter metal wires. Up till this time there have been no failures of microtubes due to internal pressurization. The initial concern was to keep the microtube geometry straight and uniform, so that bending stresses could be avoided. Improved manufacturing techniques have subsequently solved this problem.

REFERENCES

1. Schlicting, Hermann, Boundary Layer Theory, 7th Ed., McGraw Hill Book Co, NY, 1979, pp. 11.

2. Kaye, G. and Laby, T., Tables of Physical and Chemical Constants, 13th Ed., Longmans Green & Co. Ltd., 1966, pp. 35.

APPENDIX A

SAMPLE STRESS-STRAIN DATA FOR MICROTUBES

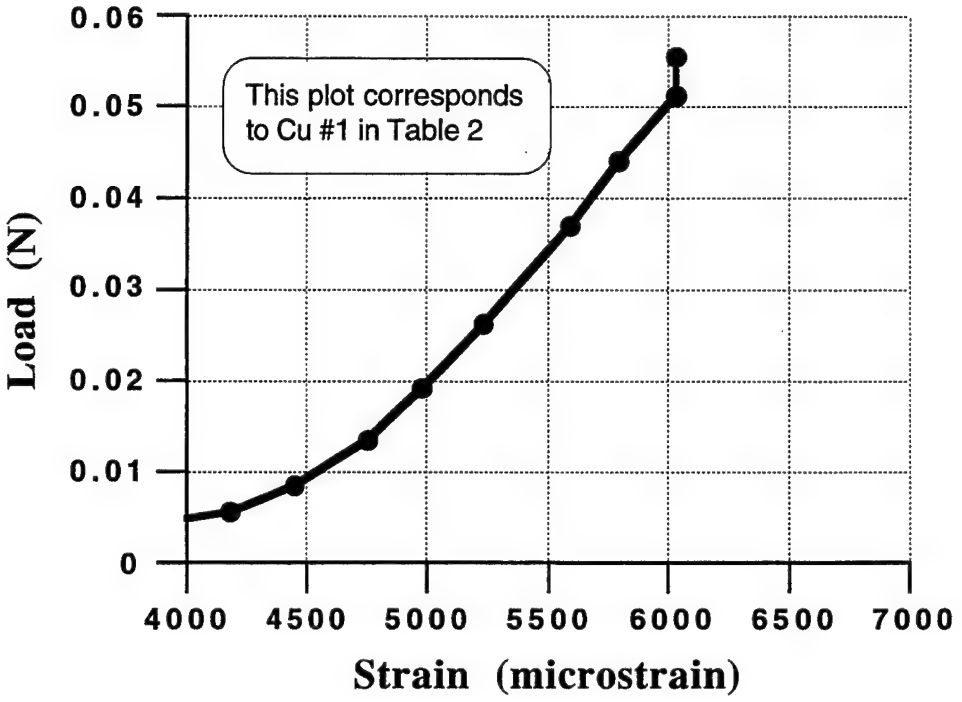

Figure A-1 : Tensile Test of Cu Microtube #1

Calculations for a straight line fitted to the upper portion of the stress-strain curve :

$$\text{slope} = \frac{0.06\ \text{N}}{(6325 - 4372) \times 10^{-6}} = EA = 30.72\ \text{N}$$

$$E_{copper} = 12.98 \times 10^{10}\ \text{N/m}^2$$

$$\text{Therefore area } A = (EA) / E_{copper} = 2.367 \times 10^{-10}\ \text{N/m}^2$$

$$\text{Ultimate Stress} = \text{Breaking load} / (\text{area A}) = 2.34 \times 10^{8}\ \text{N/m}^2$$

This is 75-84% of the tensile strength of annealed copper wire.

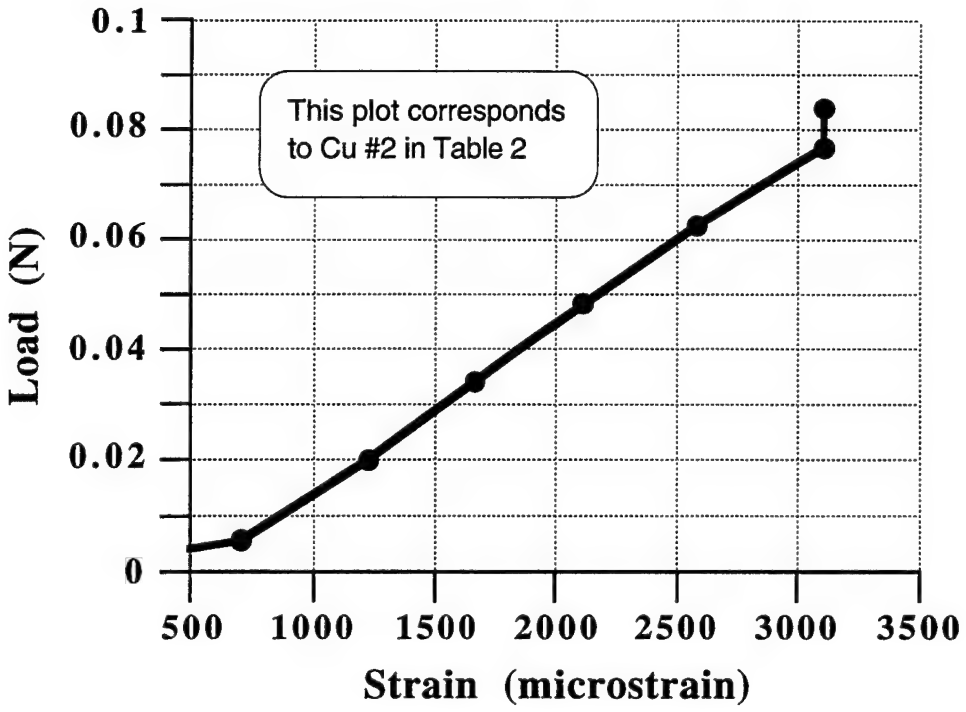

Figure A-2 : Tensile Test of Cu Microtube #2

Calculations for a straight line fitted to the upper portion of the stress-strain curve :

$$\text{slope} = \frac{0.09\ \text{N}}{(3372 - 581) \times 10^{-6}} = EA = 32.25\ \text{N}$$

$$E_{copper} = 12.98 \times 10^{10}\ \text{N/m}^2$$

$$\text{Therefore area } A = (EA) / E_{copper} = 2.485 \times 10^{-10}\ \text{N/m}^2$$

$$\text{Ultimate Stress} = \text{Breaking load} / (\text{area A}) = 3.37 \times 10^{8}\ \text{N/m}^2$$

This is 108-120% of the tensile strength of annealed copper wire.

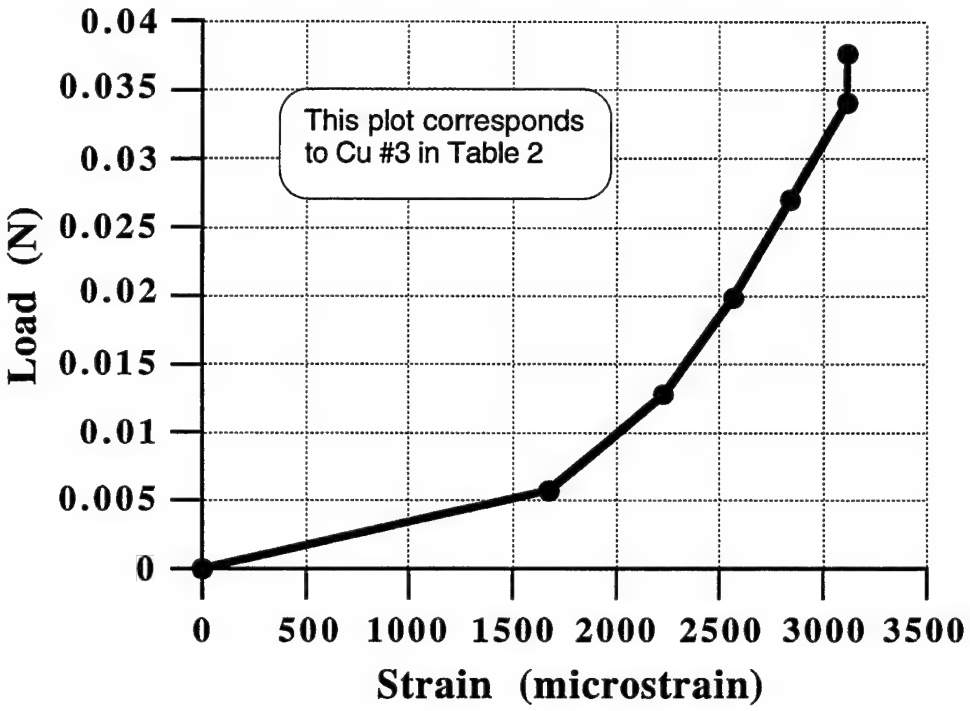

Figure A-3 : Tensile Test of Cu Microtube #3

Calculations for a straight line fitted to the upper portion of the stress-strain curve :

$$\text{slope} = \frac{0.04\ \text{N}}{(3338 - 1870) \times 10^{-6}} = EA = 27.25\ \text{N}$$

$$E_{copper} = 12.98 \times 10^{10}\ \text{N/m}^2$$

$$\text{Therefore area } A = (EA) / E_{copper} = 2.099 \times 10^{-10}\ \text{N/m}^2$$

$$\text{Ultimate Stress} = \text{Breaking load} / (\text{area A}) = 1.79 \times 10^{8}\ \text{N/m}^2$$

This is 57.7-64% of the tensile strength of annealed copper wire.

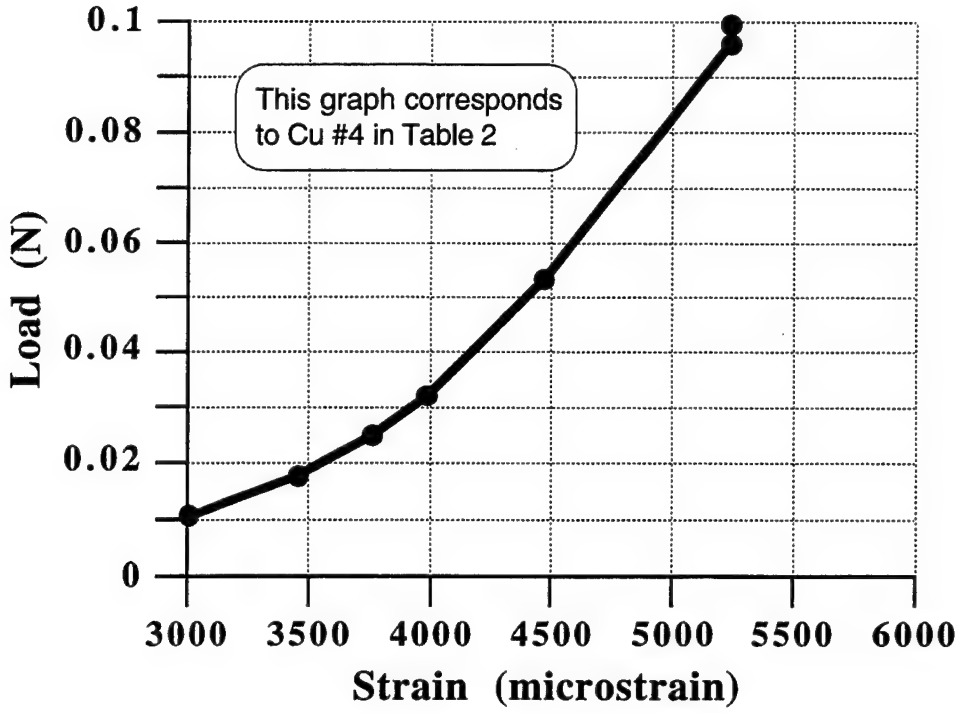

Figure A-4 : Tensile Test of Cu Microtube #4

Calculations for a straight line fitted to the upper portion of the stress-strain curve :

$$\text{slope} = \frac{0.01\ \text{N}}{(5314 - 3500) \times 10^{-6}} = EA = 55.13\ \text{N}$$

$$E_{copper} = 12.98 \times 10^{10}\ \text{N/m}^2$$

$$\text{Therefore area } A = (EA) / E_{copper} = 4.247 \times 10^{-10}\ \text{N/m}^2$$

$$\text{Ultimate Stress} = \text{Breaking load} / (\text{area A}) = 2.34 \times 10^{8}\ \text{N/m}^2$$

This is 75.6-83.6% of the tensile strength of annealed copper wire.

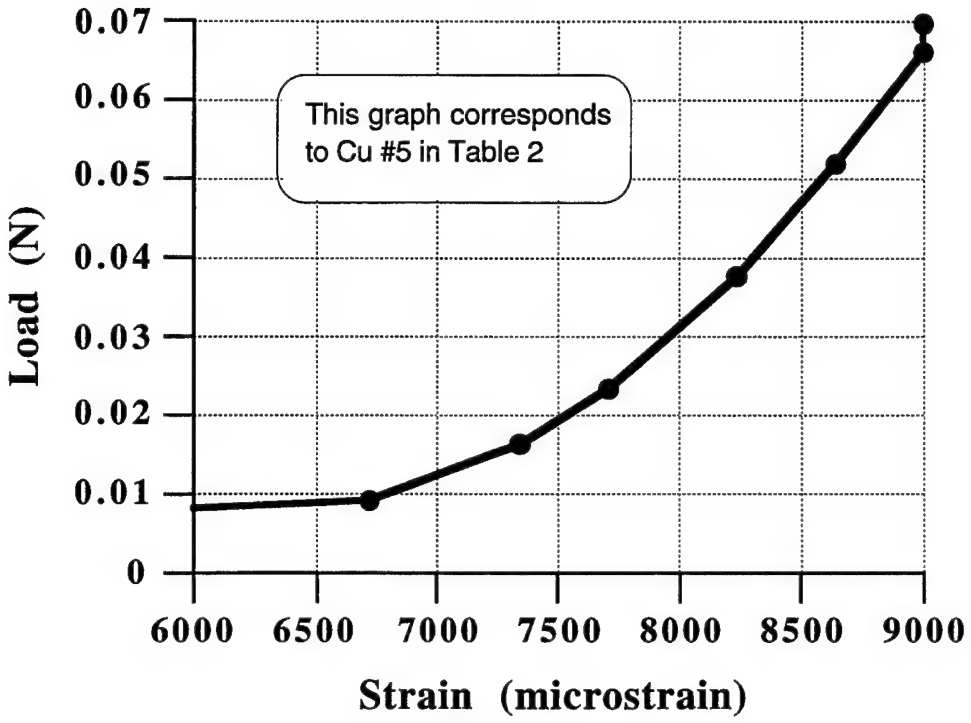

Figure A-5 : Tensile Plot of Cu Microtube #5

Calculations for a straight line fitted to the upper portion of the stress-strain curve :

$$\text{slope} = \frac{0.067\ \text{N}}{(9000 - 7250) \times 10^{-6}} = EA = 38.28\ \text{N}$$

$$E_{copper} = 12.98 \times 10^{10}\ \text{N/m}^2$$

$$\text{Therefore area } A = (EA) / E_{copper} = 2.949 \times 10^{-10}\ \text{N/m}^2$$

$$\text{Ultimate Stress} = \text{Breaking load} / (\text{area A}) = 2.36 \times 10^{8}\ \text{N/m}^2$$

This is 76-84% of the tensile strength of annealed copper wire.

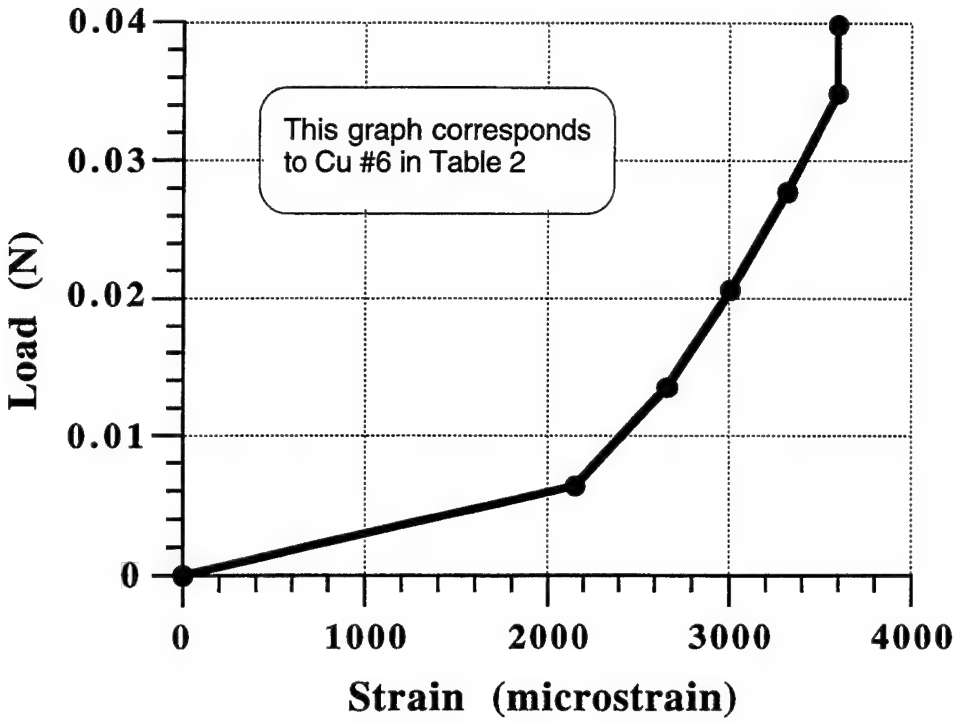

Figure A-6 : Tensile Plot of Cu Microtube #6

Calculations for a straight line fitted to the upper portion of the stress-strain curve :

$$\text{slope} = \frac{0.04\ \text{N}}{(3800 - 2195) \times 10^{-6}} = EA = 24.92\ \text{N}$$

$$E_{copper} = 12.98 \times 10^{10}\ \text{N/m}^2$$

$$\text{Therefore area } A = (EA) / E_{copper} = 1.92 \times 10^{-10}\ \text{N/m}^2$$

$$\text{Ultimate Stress} = \text{Breaking load} / (\text{area A}) = 2.07 \times 10^{8}\ \text{N/m}^2$$

This is 67-74% of the tensile strength of annealed copper wire.

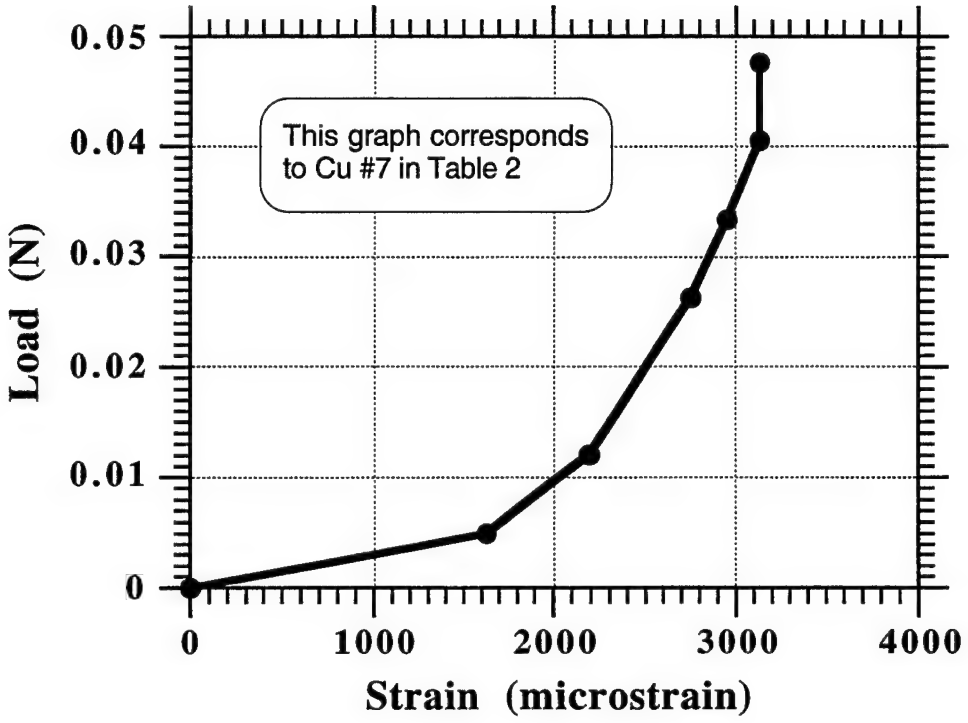

Figure A-7 : Tensile Plot of Copper Microtube #7

Calculations for a straight line fitted to the upper portion of the stress-strain curve :

$$\text{slope} = \frac{0.05\ \text{N}}{(3390 - 2050) \times 10^{-6}} = EA = 37.31\ \text{N}$$

$$E_{copper} = 12.98 \times 10^{10}\ \text{N/m}^2$$

$$\text{Therefore area } A = (EA) / E_{copper} = 2.87 \times 10^{-10}\ \text{N/m}^2$$

$$\text{Ultimate Stress} = \text{Breaking load} / (\text{area A}) = 1.66 \times 10^{8}\ \text{N/m}^2$$

This is 54-59% of the tensile strength of annealed copper wire.

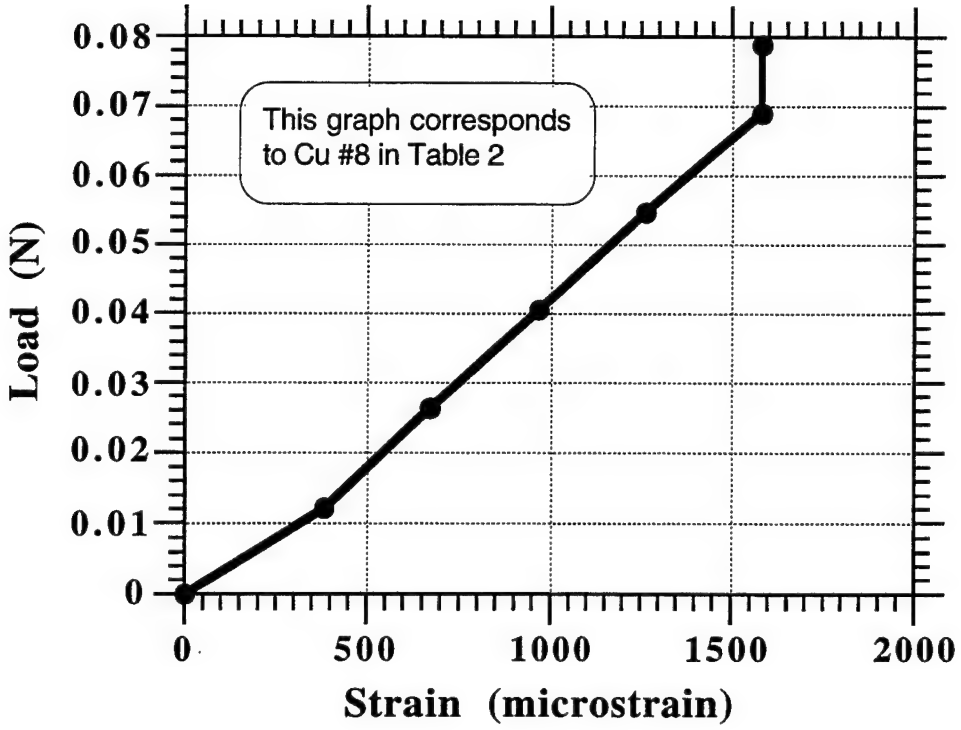

Figure A-8 : Tensile Plot of Copper Microtube #8

Calculations for a straight line fitted to the upper portion of the stress-strain curve :

$$\text{slope} = \frac{0.08\ \text{N}}{(1805 - 110) \times 10^{-6}} = EA = 47.2\ \text{N}$$

$$E_{copper} = 12.98 \times 10^{10}\ \text{N/m}^2$$

$$\text{Therefore area } A = (EA) / E_{copper} = 3.64 \times 10^{-10}\ \text{N/m}^2$$

$$\text{Ultimate Stress} = \text{Breaking load} / (\text{area A}) = 2.17 \times 10^{8}\ \text{N/m}^2$$

This is 70-78% of the tensile strength of annealed copper wire.

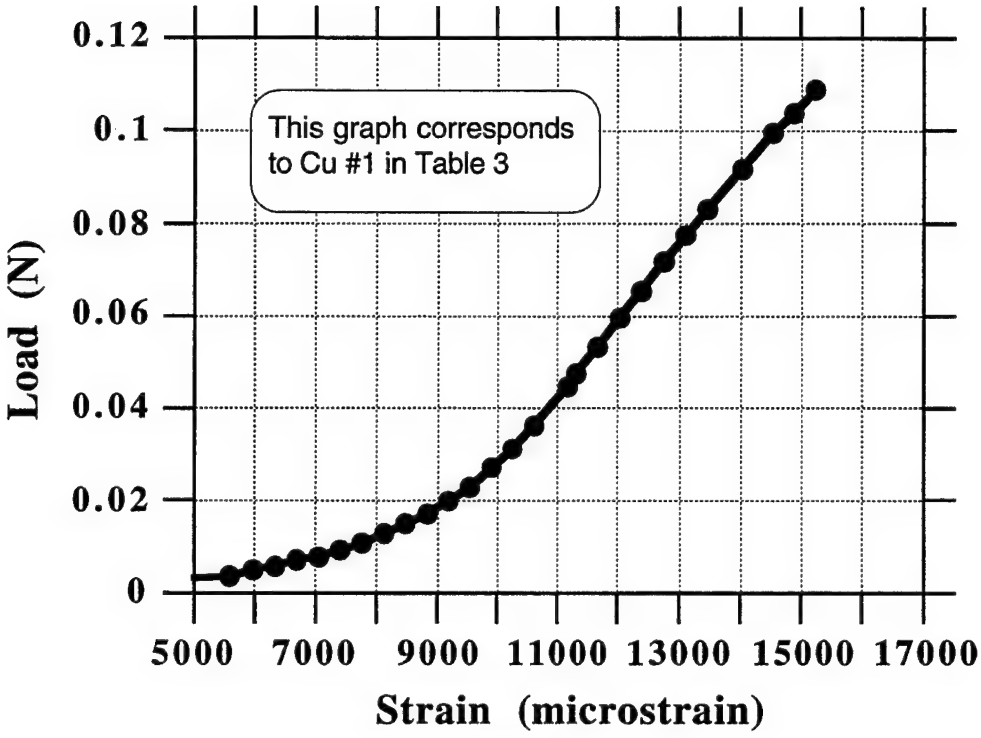

Figure A-9 : Tensile Plot of Cu Microtube #1

Calculations for a straight line fitted to the upper portion of the stress-strain curve :

$$\text{slope} = \frac{0.12\ \text{N}}{(15500 - 8400) \times 10^{-6}} = EA = 16.90\ \text{N}$$

$$E_{copper} = 12.98 \times 10^{10}\ \text{N/m}^2$$

$$\text{Therefore area } A = (EA) / E_{copper} = 1.302 \times 10^{-10}\ \text{N/m}^2$$

$$\text{Ultimate Stress} = \text{Breaking load} / (\text{area A}) = 8.35 \times 10^{8}\ \text{N/m}^2$$

This is 278% of the tensile strength of annealed copper wire.

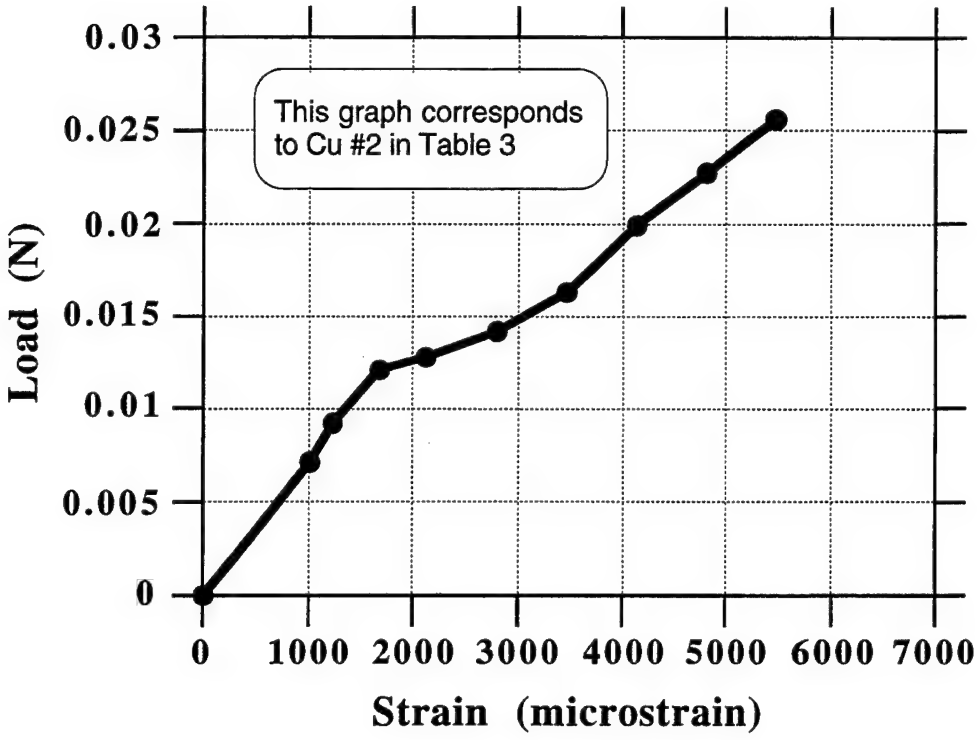

Figure A-10 : Tensile Plot of Cu Microtube #2

Calculations for a straight line fitted to the upper portion of the stress-strain curve :

$$\text{slope} = \frac{0.03\ \text{N}}{(6300 + 200) \times 10^{-6}} = EA = 4.62\ \text{N}$$

$$E_{copper} = 12.98 \times 10^{10}\ \text{N/m}^2$$

$$\text{Therefore area } A = (EA) / E_{copper} = 3.56 \times 10^{-10}\ \text{N/m}^2$$

$$\text{Ultimate Stress} = \text{Breaking load} / (\text{area A}) = 7.18 \times 10^{8}\ \text{N/m}^2$$

This is 239% of the tensile strength of annealed copper wire.

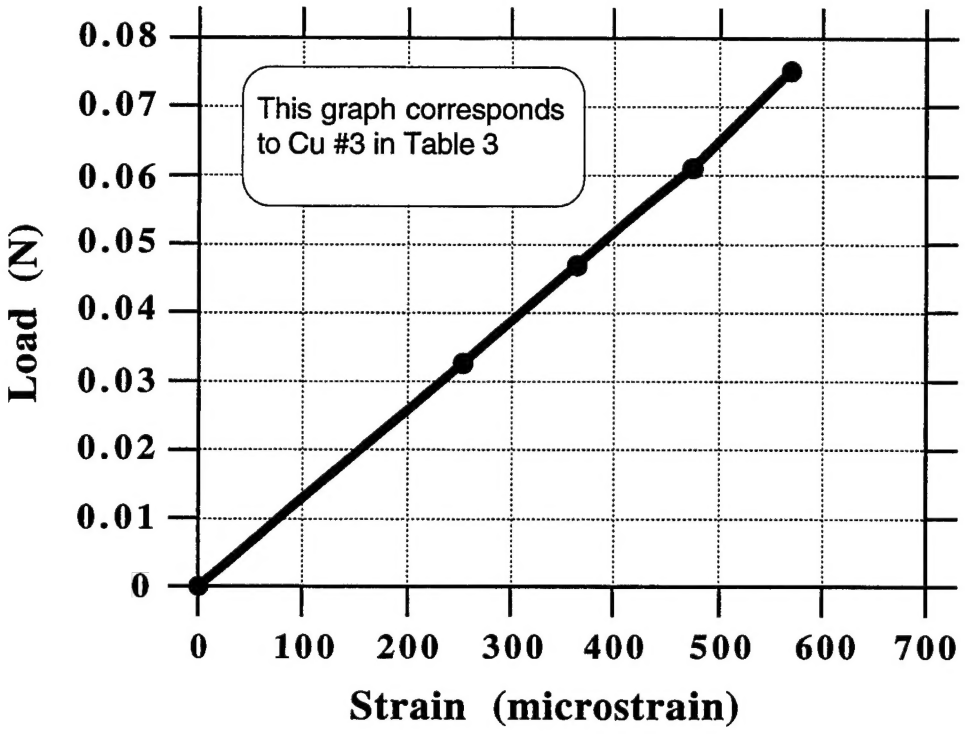

Figure A-11 : Tensile Plot of Cu Microtube #3

Calculations for a straight line fitted to the upper portion of the stress-strain curve :

$$\text{slope} = \frac{0.08\ \text{N}}{(620) \times 10^{-6}} = EA = 129.0\ \text{N}$$

$$E_{copper} = 12.98 \times 10^{10}\ \text{N/m}^2$$

$$\text{Therefore area } A = (EA) / E_{copper} = 9.94 \times 10^{-10}\ \text{N/m}^2$$

$$\text{Ultimate Stress} = \text{Breaking load} / (\text{area A}) = 0.758 \times 10^{8}\ \text{N/m}^2$$

This is 25% of the tensile strength of annealed copper wire.

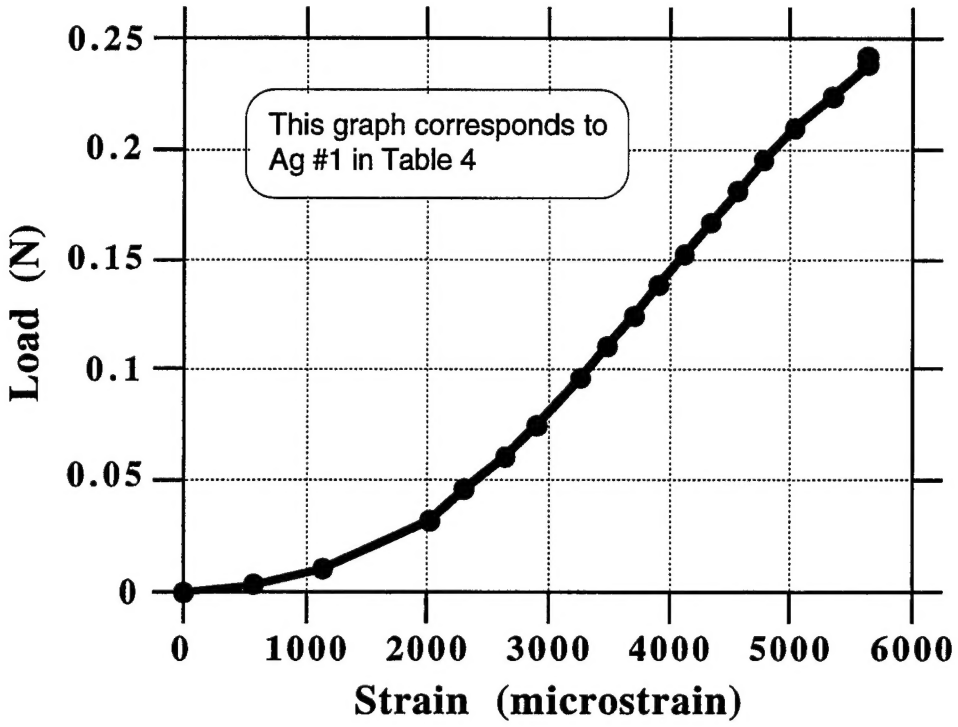

Figure A-12 : Tensile Plot of Silver Microtube #1

Calculations for a straight line fitted to the upper portion of the stress-strain curve :

$$\text{slope} = \frac{0.25\ \text{N}}{(5580 - 1800) \times 10^{-6}} = EA = 66.14\ \text{N}$$

$$E_{silver} = 8.27 \times 10^{10}\ \text{N/m}^2$$

$$\text{Therefore area } A = (EA) / E_{copper} = 8.00 \times 10^{-10}\ \text{N/m}^2$$

$$\text{Ultimate Stress} = \text{Breaking load} / (\text{area A}) = 3.02 \times 10^{8}\ \text{N/m}^2$$

This is 104% of the tensile strength of annealed silver wire.

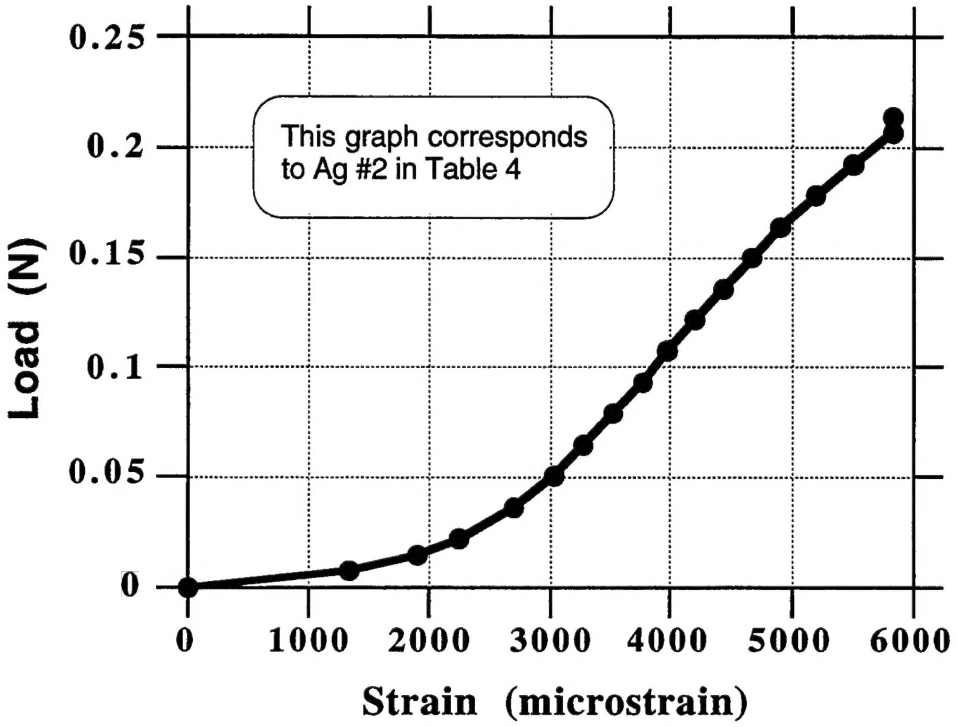

Figure A-13 : Tensile Plot of Silver Microtube #2

Calculations for a straight line fitted to the upper portion of the stress-strain curve :

$$\text{slope} = \frac{0.25\ \text{N}}{(6299 - 2225) \times 10^{-6}} = EA = 61.37\ \text{N}$$

$$E_{silver} = 8.27 \times 10^{10}\ \text{N/m}^2$$

$$\text{Therefore area } A = (EA) / E_{copper} = 7.42 \times 10^{-10}\ \text{N/m}^2$$

$$\text{Ultimate Stress} = \text{Breaking load} / (\text{area A}) = 3.26 \times 10^{8}\ \text{N/m}^2$$

This is 112% of the tensile strength of annealed silver wire.

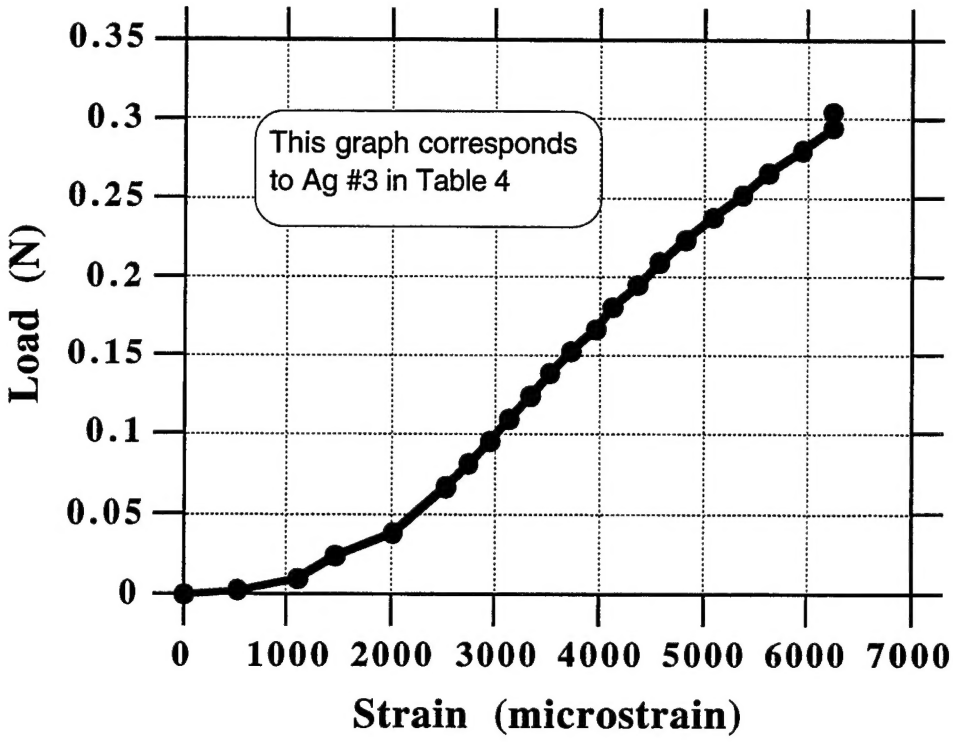

Figure A-14 : Tensile Plot of Silver Microtube #3

Calculations for a straight line fitted to the upper portion of the stress-strain curve :

$$\text{slope} = \frac{0.35\ \text{N}}{(6490 - 1600) \times 10^{-6}} = EA = 71.58\ \text{N}$$

$$E_{silver} = 8.27 \times 10^{10}\ \text{N/m}^2$$

$$\text{Therefore area } A = (EA) / E_{copper} = 8.65 \times 10^{-10}\ \text{N/m}^2$$

$$\text{Ultimate Stress} = \text{Breaking load} / (\text{area A}) = 3.52 \times 10^{8}\ \text{N/m}^2$$

This is 121% of the tensile strength of annealed silver wire.